

## Diffusing wave spectroscopy and small-angle neutron scattering from concentrated colloidal suspensions

L. F. Rojas-Ochoa,<sup>1</sup> S. Romer,<sup>1,2</sup> F. Scheffold,<sup>1,\*</sup> and P. Schurtenberger<sup>1</sup>  
<sup>1</sup>*Department of Physics, University of Fribourg, CH-1700 Fribourg, Switzerland*  
<sup>2</sup>*Polymer Institute, ETH Zurich, CH-8092 Zurich, Switzerland*

(Received 7 November 2001; revised manuscript received 12 March 2002; published 21 May 2002)

We have studied the properties of dense colloidal suspensions with a combination of small-angle neutron scattering (SANS) and diffusing wave spectroscopy (DWS). Contrary to single light scattering, DWS provides dynamic information on length scales, from 1 to 100 nm, comparable to SANS. This offers a unique range of accessible length and time scales perfectly suited for the (noninvasive) investigation of highly concentrated systems. By this we obtain valuable information about the structural properties and the short-time diffusion of electrostatically stabilized, but strongly screened, hard-sphere-like colloidal suspensions with volume fractions up to 30%. We furthermore discuss the consequences of local structural ordering on the optical properties, such as optical density and polarization. Quantitative agreement is found when comparing transmission measurements (optical density) with parameter-free numerical calculations based on the structural characterization from SANS.

DOI: 10.1103/PhysRevE.65.051403

PACS number(s): 82.70.Dd, 83.80.Hj, 42.25.Dd, 61.12.Ex

### I. INTRODUCTION

The interactions between charged colloidal particles are of fundamental importance for many questions related to the macroscopic behavior of colloidal suspensions, such as their mechanical properties or, most importantly for industrial applications, their stability against aggregation [1]. Therefore, a comprehensive knowledge of both local dynamic and static properties of colloidal suspensions is important for the description of industrially relevant systems. On the other hand, the length and time scales involved are experimentally much more accessible for colloidal suspensions than for atomic or molecular systems. This makes colloidal suspensions ideal candidates to serve as well-controlled model systems in statistical mechanics, e.g., for the study of liquids, gels, glasses, etc. [2–6].

Information about the static and dynamic properties on length scales comparable to the size of the particles is usually obtained from static and dynamic light scattering (SLS, DLS) in the single-scattering regime [7,8]. In dense suspensions, however, these powerful techniques cannot be applied in most cases due to strong multiple scattering of light. In addition, the  $q$  range [ $q = 4\pi n \sin(\theta/2)/\lambda$ ] and hence the length scales probed by standard light-scattering techniques ( $\lambda/n \approx 400$  nm) are limited to  $q < 0.03$  nm<sup>-1</sup>, further complicating its application to many concentrated systems. An elegant way to overcome this limitation is to take advantage of the multiple-scattering process rather than avoiding it. Diffusing wave spectroscopy (DWS) works in the limit of very strong multiple scattering, where a diffusion model can be used in order to describe the propagation of the light across the sample [9–11]. Using such a diffusion approximation, one can then determine the distribution of scattering

paths and calculate the temporal autocorrelation of the intensity fluctuations analogous to DLS. It is thus still possible to study the dynamics of a colloidal suspension by measuring the intensity fluctuations of the scattered light observed either in transmission or reflection. While DWS does not yield explicit information on the  $q$  dependence of the so-called dynamic structure factor  $S(q,t)$ , it is capable of providing unique information on particle motion on very short time scales. The fluctuations of the scattered light measured in transmission result from the variation of the total path length by a wavelength of light. However, since the light is scattered from a large number of particles, each individual particle must move only a small fraction of a wavelength for the cumulative change in path length to be a full wavelength. Therefore, DWS can probe particle motion on very short length scales, and it has, for example, been demonstrated that it can measure motions of particles of order 1  $\mu$ m in diameter on length scales of less than 1 nm [12,13]. In this paper, we demonstrate how a combination of DWS and small-angle neutron scattering (SANS) can provide quantitative information about the static and dynamic properties of highly screened charge-stabilized colloidal suspensions (polystyrene latex spheres). A full structural characterization is also a prerequisite to quantitatively describe (and henceforth predict) the optical properties of dense colloidal systems. As a first step towards a complete understanding of this class of materials, we compare the optical density of our model suspensions, as obtained from transmission measurements, with parameter-free numerical calculations based on the experimentally determined structure factor  $S(q)$  from SANS. Furthermore, we discuss in detail how the concentration dependence of  $S(q)$  modifies the polarization properties of multiply scattered light. We note that our general approach of combining SANS and DWS is not limited to this specific system but can be equally well applied to other soft particle systems, such as aggregating and gelling suspensions or colloidal suspensions near the glass transition. These more com-

\*Corresponding author.

Email address: Frank.Scheffold@unifr.ch

plex systems are a subject of our ongoing research activities and will be discussed in future articles [14].

## II. MATERIALS

Charge-stabilized aqueous suspensions of polystyrene spheres were prepared at different volume fractions  $\phi$ , range 0.4–30%. The samples were taken from a stock suspension of 8.2% solid weight fraction (as obtained from Interfacial Dynamics Corp., Portland, OR) to which salt was added to obtain a final ionic strength of 5 mM of KCl. At the chosen ionic strength, the electrostatic repulsion between particles is expected to be almost entirely screened with a screening length of 4 nm or less. We additionally added 2 mM of SDS to increase the stability of the suspension against aggregation. Concentrated suspensions were prepared by slow water evaporation in a dialysis tube, thereby further increasing the salt concentration and decreasing the screening length. The sample concentrations (volume fraction  $\phi$ ) were determined, with an estimated accuracy of  $\pm 2.5\%$ , by drying a known suspension amount and subsequent weighing (polystyrene density  $1.055 \times 10^{-3}$  kg/m<sup>3</sup>). Multiple neutron scattering has been suppressed by partially contrast-matching the particles using a H<sub>2</sub>O-D<sub>2</sub>O ( $\sim 40:60$ ) mixture. Small additional contrast corrections have been performed separately for every sample before each SANS measurements. However, this does not affect the particle interaction properties and the light-scattering contrast (all systems show strong multiple light scattering).

## III. STRUCTURAL PROPERTIES

### A. Small-angle neutron scattering (SANS) experiments

The structural properties of dense colloidal suspensions were studied using small-angle neutron scattering at the Swiss neutron source at the Paul Scherrer Institute.<sup>1</sup> We present a systematic comparison of the static properties of such systems, characterized by the  $q$ -dependent neutron scattering intensity, to the theoretical predictions for suspensions of hard spheres, as obtained from integral equations theory [15]. The measurements were performed with a mean neutron wavelength of 1.68 nm and at a detector distance of 18 m, which corresponds to the  $q$  range of 0.01–0.1 nm<sup>-1</sup>. The scattered neutron intensity was recorded with a two-dimensional (2D) neutron detector. The initial data treatment and the data analysis were performed as described in [16]. The samples were kept in stoppered quartz cells (Hellma, Germany) with a path length of 1 mm. The neutron spectra of water were also measured in a 1-mm path-length quartz cell. The raw spectra were corrected for background from the solvent, sample cell, and electronic noise by conventional procedures. Furthermore, the two-dimensional isotropic scattering spectra were azimuthally averaged, converted to absolute scale, and corrected for detector efficiency by dividing with the incoherent scattering spectra of pure water [17–20].

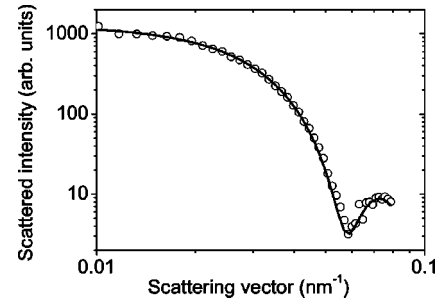


FIG. 1. Neutron scattering intensity for the  $\phi=0.4\%$  sample. The solid line shows the best fit using the form factor for spherical particles with  $a=79.8$  nm.

The smearing induced by the instrumental setup is included in the data analysis discussed below. The ideal model scattering curves were smeared by the appropriate resolution function when the model scattering intensity was compared to the measured one [21,22]. The parameters in the models were optimized by conventional least-squares analysis, and the errors of the parameters were calculated by conventional methods [23].

### B. Results

Figures 1 and 2 show the results obtained from measurements at samples with different solid content. The measured intensity  $I(q)$  as a function of the scattering vector  $q$  contains contributions from the particle structure [SANS particle form factor  $F(q)$ ] as well as from interparticle interaction effects [structure factor  $S(q)$ ],  $I(q) \propto F(q)S(q)$ .  $F(q)$  can be determined experimentally from a dilute suspension as shown in Fig. 1. We have used a 0.4% dispersion and the result has been fitted using a polydisperse form factor convoluted with the instrumental resolution (see inset of Fig. 2). On that basis, we determine a particle radius of  $a=79.8$  nm and a polydispersity of about 3% (supplier specification: radius 85 nm, intrinsic polydispersity, 4%).

Figure 2 shows the corresponding scattering intensity for the  $\phi=0.12\%$ ,  $\phi=0.15\%$ ,  $\phi=0.25\%$ , and  $\phi=0.3\%$  samples. In all cases, the experimental data are found in excellent agreement with the theoretical prediction based on integral equations theory using the Percus-Yevick closure relation derived for a suspension of hard spheres [15]. The only adjustable parameter in our fitting procedure is the sample volume fraction  $\phi_{\text{eff}}$ , which is found in good agreement with the values obtained from drying and weighing (Fig. 2).

## IV. OPTICAL DENSITY—THE INVERSE TRANSPORT MEAN FREE PATH

The optical density  $1/l^*$  is a key quantity to characterize random media. For a given system size, it separates the regime of diffuse light propagation from moderate or weak scattering. This means that if the system dimensions are much larger than  $l^*$ , it is optically dense and the transmission of unscattered light is suppressed. With further increasing optical density, deviations from the simple picture of

<sup>1</sup>Villigen, Switzerland, <http://sinq.web.psi.ch/>

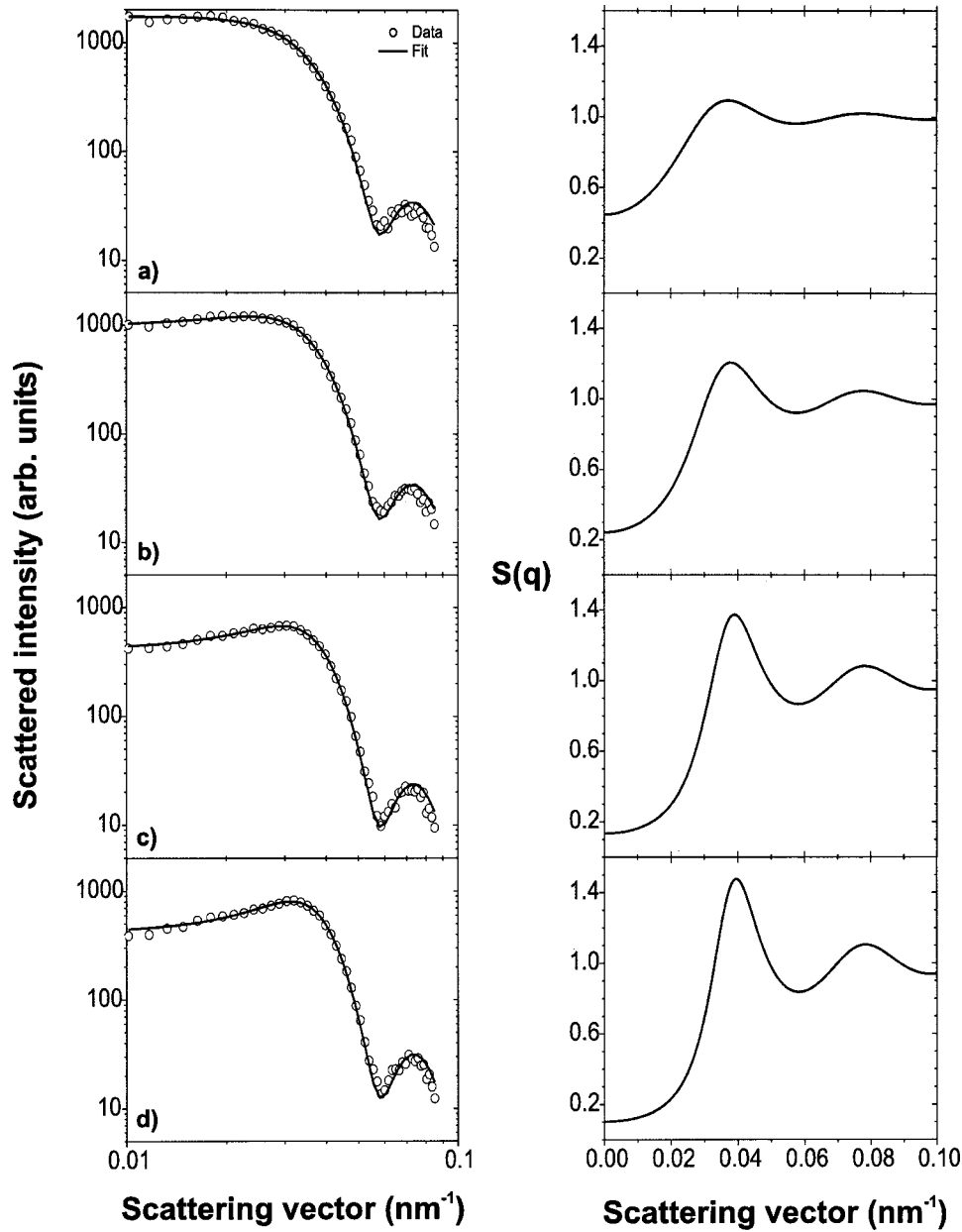


FIG. 2. Neutron scattering intensity  $I(q)$  and static structure factor  $S(q)$ . The latter was obtained by fitting the PY-structure factor (hard spheres, convoluted by the system resolution) with an effective concentration  $\phi_{\text{eff}}$  to the SANS intensity as shown by the solid lines on the left-hand side (for details see text). The figure shows the results for different volume fractions: (a)  $\phi=0.12$  ( $\phi_{\text{eff}}=0.103$ ), (b)  $\phi=0.15$  ( $\phi_{\text{eff}}=0.181$ ), (c)  $\phi=0.25$  ( $\phi_{\text{eff}}=0.256$ ), and (d)  $\phi=0.3$  ( $\phi_{\text{eff}}=0.289$ ).

diffuse light propagation appear [24,26,25] until at  $k_0 l^* \approx 1$  (Ioffe-Regel criterion [26]) a complete breakdown of classical transport theory is expected; light cannot propagate any more due to strong Anderson localization [26–28]. Despite this importance, only a few studies have addressed the question of how interparticle interactions influence  $l^*$  [29–31]. In this paper, we present, to our knowledge, the first study where all system parameters have been determined independently in order to predict theoretically the optical density of a sample. In the following section, we will briefly review the existing theoretical models. Subsequently, we describe the experimental procedure and compare both theory and experiment. Note that our particles are much smaller than the

wavelength of light and therefore we expect a pronounced influence of structural correlations on the optical density.

#### A. Photon diffusion in suspensions of hard spheres

Light propagation in disordered materials is determined by the scattering of the individual particles (or in more general terms the variation in the refractive index), for spherical particles given by the Mie scattering function  $P(q) = k_0^2 (d\sigma_{\text{sc}}/d\Omega)$  [32], the particle number density  $\rho = \phi/(4\pi a^3/3)$ , and interparticle correlations characterized by  $S(q)$ . For dilute noninteracting systems [ $S(q) \equiv 1$ ], the optical properties can be characterized by the scattering mean free path [33],

$$l = \frac{1}{\rho \frac{2\pi}{k_0^4} \int_0^{2k_0} P(q) q dq} = \frac{1}{\rho \sigma_{sc}}, \quad (1)$$

which is found inversely proportional to the total scattering cross section of a particle  $\sigma_{sc}$ . Initially this leads to an exponential decay of the unscattered intensity transmitted through a slab of thickness  $L$ :  $T_0 = \exp(-L/l)$ . With increasing density, multiple scattering contributions become important until in the case of strongly turbid systems light propagates diffusively, hence  $T \propto l^*/L$ . The typical length characterizing the diffusion process is the transport mean free path  $l^*$ , which can be written quite generally in terms of the mean-square scattering vector [11],

$$\frac{l^*}{l} = \frac{1}{1 - \langle \cos \theta \rangle} = \frac{2k_0^2}{\langle q^2 \rangle}. \quad (2)$$

$\langle \rangle$  denotes the angular average over all scattering angles  $\theta$ , weighted by the scattering probability. For dilute systems, the scattering probability is simply given by the differential cross-section or single-particle scattering function  $P(q)$ . Positional correlations between particles affect dramatically the optical density of concentrated colloidal suspensions because they change the angular distribution of scattered light emerging from each scattering event and therefore change the value of  $l^*$ . For correlated systems we replace  $P(q)$  with the full scattering function  $P(q)S(q)$ ; thus we obtain

$$\langle q^2 \rangle = \frac{\int_0^{2k_0} P(q)S(q)q^3 dq}{\int_0^{2k_0} P(q)S(q)q dq} \quad (3)$$

or

$$\frac{l^*}{l} = 2k_0^2 \frac{\int_0^{2k_0} P(q)S(q)q dq}{\int_0^{2k_0} P(q)S(q)q^3 dq}. \quad (4)$$

Therefore, the general expression for  $l^*$  in a correlated suspension of spherical particles reads [29]

$$l^* = k_0^6 \left( \pi \rho \int_0^{2k_0} P(q)S(q)q^3 dq \right)^{-1}. \quad (5)$$

## B. Experiments and results

To determine the concentration dependence of  $l^*$ , we measured the transmitted intensities  $T$  through a slab for the samples of interest relative to reference samples,  $T_S$ , of known  $l_S^*$ . Thus the ratio of transmitted intensities directly yields the unknown  $l^*$  [34],

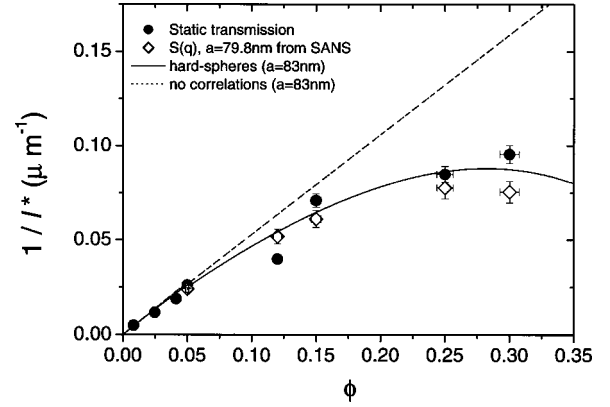


FIG. 3. Inverse of the transport mean free path  $1/l^*$  as a function of the volume fraction  $\phi$ . Circles: data obtained from static transmission measurements. The lines show the theoretical predictions for a suspension of hard spheres of radius 83 nm [dashed line, without interactions  $S(q) = 1$ ; solid line, with correlations modeled with the PY static structure factor]. The parameter free predictions from the SANS measurements are shown as diamonds [Eq. (5) with  $a = 79.8$  nm,  $S(q)$  from SANS].

$$\frac{T}{T_S} = \frac{l^*}{l_S^*} \frac{\left(1 + \frac{4}{3} \frac{l_S^*}{L}\right)}{\left(1 + \frac{4}{3} \frac{l^*}{L}\right)}. \quad (6)$$

Figure 3 displays the determined values of  $1/l^*$  as well as the theoretical predictions. Quantitative agreement is found between theory and experiment. For the parameter-free SANS calculations, we have considered a particle size  $a = 79.8$  nm (see Sec. III B) for the calculation of  $P(q)$  leading to slightly lower values of  $1/l^*$ .

## V. DYNAMICS

### A. Particle motion in a dense suspension of hard spheres

In the classical DLVO theory [35], for charged particles the (kinetic) stability is explained by assuming that a repulsive, Debye-Hückel-type interaction superimposes to the attractive van der Waals interaction, resulting in a net repulsion between like charged particles if charges are sufficiently large and the screening by the surrounding electrolyte is not too strong. The dynamic properties on short length scales are then usually discussed in terms of an effective short time diffusion coefficient  $D_s$ . For sufficiently short-times the random diffusive motion of a colloidal particle in a solvent of known viscosity  $\eta$  is therefore fully characterized by its mean-square displacement,  $\Delta r^2(t) = 6D_s t$ . For dilute and noninteracting systems,  $D_s$  reduces to the free diffusion coefficient given by the Stokes-Einstein relation [1],

$$D_0 = \frac{k_B T}{6\pi\eta a}, \quad (7)$$

where  $a$  is the particle (hydrodynamic) radius.  $D_0$  can be measured in a dynamic light-scattering (DLS) experiment

where the relaxation time of the exponentially decaying field autocorrelation function  $g_1(t)$  is given by [8]

$$\tau_0 = \frac{1}{D_0 q^2}. \quad (8)$$

In concentrated systems it has been shown that the particle dynamics is still diffusive. Structural correlations and hydrodynamic interactions, however, influence this diffusion process. Taking this into account, we can express the effective  $q$ -dependent diffusion coefficient in the following terms [7]:

$$D_{\text{eff}}(q) = D_0 \frac{H(q)}{S(q)}. \quad (9)$$

The influence of interparticle interactions on the particle dynamics is described by  $D_{\text{eff}}(q) = D_s h(q)/S(q)$ , with  $h(q) = H(q)/H(\infty)$ .  $D_s = D_0 H(\infty)$  denotes the short-time self-diffusion coefficient. We used the Beenakker-Mazur formalism [36] to calculate  $h(q)$  and, in that way, include hydrodynamic interactions in our analysis. The static structure factor was taken from the independent SANS measurements as described above, which leaves our analysis free of any adjustable parameters. Rather than using the core size obtained from SANS, we use the hydrodynamic radius of the particles for our dynamic analysis, which has been determined independently by DLS [7] of a highly diluted suspension to  $a = 83 \pm 2$  nm. We can therefore fully predict the short-time self-diffusion coefficient for our hard-sphere-like systems, without any adjustable parameters. In the following section, we will compare these predictions with experimental results obtained from a dynamic multiple light-scattering analysis.

### B. Diffusing wave spectroscopy—DWS

DWS [10,11,29] is an extension of DLS to the limit of strong multiple scattering. Both techniques are based on the analysis of fluctuations of the scattered light intensity in a localized spatial region (speckle). The fluctuations reflect the internal dynamics of the scattering medium and can be characterized by their normalized field autocorrelation function  $g_1(t)$ . For ergodic systems, the field autocorrelation function is linked to the intensity autocorrelation function through the Siegert relation  $g_2(t) - 1 = \langle I(0)I(t) \rangle / \langle I(0) \rangle^2 - 1 = |g_1(t)|^2$ . In transmission geometry (plane-wave illumination) [11,37],

$$g_1(t) \cong \frac{(L/l^* + 4/3) \sqrt{6t/\tau}}{\sinh[(L/l^* + 4/3) \sqrt{6t/\tau}]}. \quad (10)$$

If the interparticle structure factor  $S(q)$  is known, we can relate  $\tau$  directly to the short-time diffusion coefficient  $D_s = D_0 H(\infty)$  via an integral expression [29,38],

$$\frac{\tau}{\tau_0} = \frac{[S]}{[H]} = \frac{\int_0^{2k_0} P(q)S(q)q^3 dq}{\int_0^{2k_0} P(q)H(q)q^3 dq} = \frac{D_0}{D_s} R, \quad (11)$$

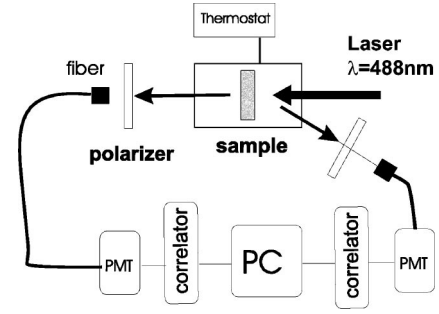


FIG. 4. Diffusing wave spectroscopy (DWS) experimental setup. An expanded, polarized laser beam ( $\lambda = 488$  nm) is incident on a sample cell immersed in a temperature-controlled water bath ( $T = 22$  °C). Temporal fluctuations are detected either in transmission or backscattering (with a polarizer) using single-mode (SM) fibers. The intensity fluctuations are subsequently analyzed with a photomultiplier and a digital correlator.

with

$$R = \frac{\int_0^{2k_0} P(q)S(q)q^3 dq}{\int_0^{2k_0} P(q)h(q)q^3 dq}, \quad (12)$$

$\tau_0 = (D_0 k_0^2)^{-1}$ ,  $k_0 = 2\pi n/\lambda$  is the wave number,  $n$  is the solvent refractive index,  $\lambda$  the laser wavelength in vacuum, and  $P(q)$  is the Mie scattering function  $P(q) = k_0^2 (d\sigma_{\text{sc}}/d\Omega)$  [32,39]. This expression, which we evaluate numerically, takes into account both the influences of structural correlations,  $S(q)$ , and hydrodynamic interactions,  $h(q) = H(q)/H(\infty)$ , which makes an *ad hoc* estimation of the concentration dependence of  $\tau$  difficult.

### C. Experiments and results

In our DWS setup, the sample cell is mounted into a water bath which serves as a temperature-control reservoir ( $T = 22$  °C) as shown in Fig. 4. Furthermore the water significantly reduces total internal reflection at the sample cell wall. A polarizer and  $\lambda$  half-wave plate setup (not shown) allows a continuous variation of the incident light intensity coming from an Ar<sup>+</sup> laser at a wavelength of  $\lambda = 488$  nm. The beam has been expanded to a diameter of about 7 mm. The samples at higher concentrations are identical to those used in the SANS experiments. For concentrations  $\phi < 10\%$ , we have used cells of different thickness such that  $L/l^* \geq 20$  for all samples, thus ensuring the validity of the diffusion approximation [9–11]. We have measured the intensity correlation function in transmission geometry for different concentration ranging from 1% to 30%. In Fig. 5(a), we plot the decay time  $\tau$  relative to its value at low concentration  $\tau_0$ , obtained from a fit of the data to Eq. (10). We then compare the experimental results to a parameter-free model calculation using the Percus-Yevick static structure factor  $S(q)$  obtained from the SANS measurements, the Mie [32] scattering function  $P(q)$ , and the Beenakker-Mazur hydrodynamic function  $h(q)$  [36,40]. Excellent agreement between theory

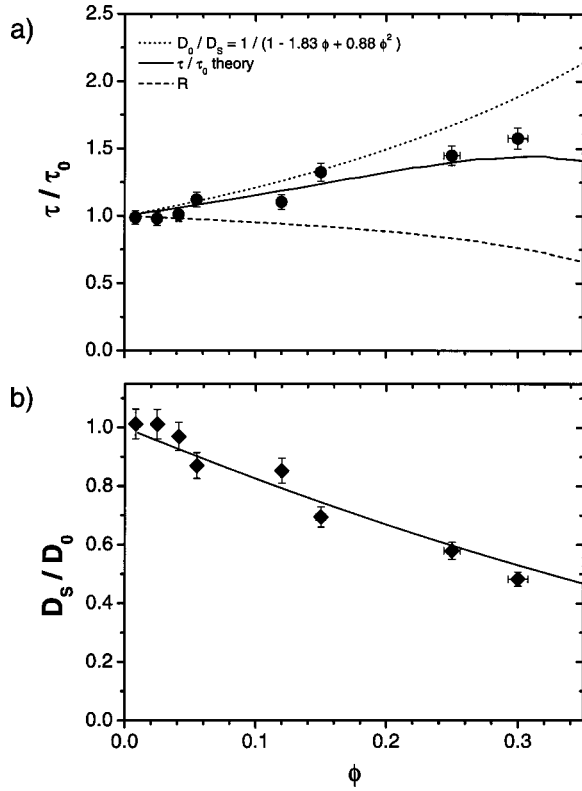


FIG. 5. (a) Concentration dependence of the relaxation time  $\tau$ . The solid line represents the theoretical prediction for hard spheres, Eq. (11). The  $R(\phi)$  contribution in Eq. (11) stems from the modified light propagation in correlated suspensions while  $D_0/D_s(\phi)$  reflects the slowed down particle diffusion. (b) Ratio of the diffusion coefficients  $D_s(\phi)/D_0 = \tau_0 R(\phi)/\tau$  vs  $\phi$ . The solid line shows the virial expansion of  $D_s(\tau_0 R(\phi)/\tau)$  for hard spheres, Eq. (13).

and experiment is found. For illustration purposes, we also display the integral  $R$  as a function of concentration [see Eq. (12)]. In Fig. 5(b), the corresponding diffusion coefficients are shown, as obtained by dividing the measured values of  $\tau/\tau_0$  with the calculated value of  $R$  at a given concentration. The experimental values of  $D_s$  follow the well-known virial expansion of the short-time diffusion coefficient [41],

$$\frac{D_s(\phi)}{D_0} = 1 - 1.83\phi + 0.88\phi^2. \quad (13)$$

Note that this experimental approach can be used quite generally to obtain model-free information about the colloidal dynamics at elevated concentrations. In the above analysis, we have considered the stationary hydrodynamic function  $h(q)$  as an input to calculate the short-time self-diffusion constant  $D_s(\phi)$  from the experimental data. In a more general approach, described in detail in Ref. [42], the dynamic properties of dense colloidal systems (suspensions, glasses, gels, etc.) can be accessed directly from the measured correlation function provided  $S(q)$  is known. For very short correlation times, the full ( $q$ -averaged) time evolution of the hydrodynamic function  $[H(t)]$  can be studied by DWS [42,40].

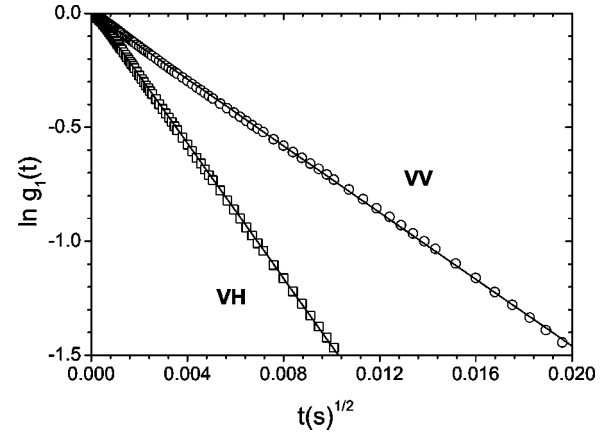


FIG. 6. Field autocorrelation function from DWS in backscattering geometry for  $\phi = 25\%$ . From a fit to the linear slope of  $\ln g_1(t)$  as a function of  $t^{1/2}$ , the values of  $\gamma_{VH}$  and  $\gamma_{VV}$  are obtained.

## VI. DEPOLARIZATION OF LIGHT IN CORRELATED SUSPENSIONS

Multiply scattered light can also be detected in reflection (backscattering) geometry where the following expression (incident plane wave) describes well the measured correlation functions ( $L \gg l^*$ ) [11]:

$$g_{(1)}(t) \cong e^{-\gamma\sqrt{6t/\tau}}. \quad (14)$$

In a scalar theory of diffuse wave propagation, the constant  $\gamma \approx \frac{5}{3}$  takes into account the coupling of the incident light to the diffuse propagation inside the medium [43,44]. However, initially linearly polarized light reflected from a turbid medium comprises a fair amount of light scattered along short paths  $s \approx l^*$ . Such short paths preserve polarization to a large extent since polarization of the scattered light is lost exponentially with  $n = s/l + 1$  [11,45,46].

In DWS experiments, it was found that this *polarization memory* influences the value of  $\gamma$  but does not significantly alter the functional shape of the correlation function, Eq. (14) [11]. In an experiment, the different components of vertical (VV) and horizontal (VH) polarization states can be detected separately (VV detection measures the polarization-conserving component of the scattered light). Previous experiments have addressed the influence of the particle size on  $\gamma_{VH, VV}$  [11,45–47]. It was found that the polarization properties of reflected light are connected to the characteristics of the single-scattering process: small (Rayleigh) particles scatter isotropically ( $l^* \cong l$ ) and light leaves the sample with a high degree of polarization after only a few scattering events. In contrast, for large (Mie) particles ( $l^*/l > 10$ ) many scattering events occur already for paths of length  $s \approx l^*$ , which leads overall to an almost full depolarization of the reflected light.

Using our well characterized system of small (almost Rayleigh-like) colloidal particles, we have addressed the issue of how interparticle correlations influence the depolarization of multiply scattered light. Such information is valuable since in practice (e.g., for applications in particle sizing or process monitoring, see, e.g., [11,48]) the systems are often

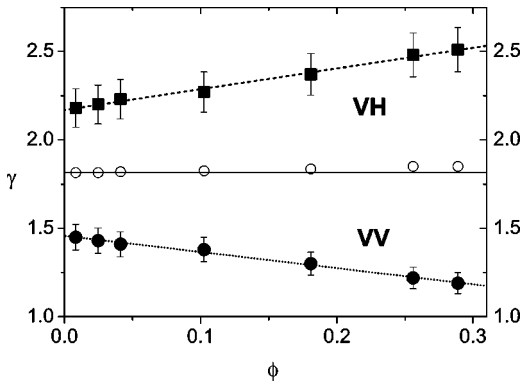


FIG. 7. Solid symbols: concentration dependence of  $\gamma_{VH}$  and  $\gamma_{VV}$  (dashed lines are a guide to the eyes only). The average  $\langle \gamma \rangle = (\gamma_{VH} + \gamma_{VV})/2$  (open circles) is found almost constant [solid line,  $\langle \gamma(\phi=0) \rangle = 1.815$ ].

highly concentrated, and without any knowledge of  $\gamma$  an accurate analysis of the local colloidal dynamics is impossible [note that the value of  $\gamma$  enters quadratically the analysis of  $\tau$  in Eq. (14)]. As a first step towards an understanding of the complex interplay between structural ordering and depolarization of light, we have measured the correlation function in backscattering geometry for both detection states, Fig. 6. The corresponding results for  $\gamma$  (Fig. 7) display an unexpected strong concentration dependence of  $\gamma$ . As a matter of fact, the difference between  $\gamma_{VH}$  and  $\gamma_{VV}$  increases continuously with increasing concentration. Such a behavior can be understood qualitatively based on the concentration dependence of  $S(q)$  shown in Fig. 2. Increasing short-range structural order [ $S(q)$ ] leads to a lower scattering intensity at low  $q$  (i.e., forward scattering). The value of  $l^*/l$ , given by Eq. (4), is thereby reduced until it becomes even smaller than 1 for concentrations above  $\phi = 22\%$ . Hence on average light is now scattered slightly backwards at each single scattering event: for a given path length  $s/l^*$  [with  $s/l^* = (s/l)(l/l^*) = (n-1)(l/l^*)$ ] it now takes fewer scattering events  $n$  and therefore the degree of remaining polarization is higher. Also note our experimental finding, Fig. 7, that the average value  $\langle \gamma \rangle = (\gamma_{VH} + \gamma_{VV})/2$  is almost constant over the whole concentration range explored. This may serve as a basis for the dynamic analysis of colloidal systems with DWS if a more detailed knowledge of  $\gamma_{VH, VV}$  is missing. In the future, we will plan to study in more detail this interesting behavior using different particle sizes and concentrations. We hope that, based on such a comprehensive analysis, a more quantitative prediction of the polarization properties of multiply scattered light will be possible.

## VII. SUMMARY AND CONCLUSIONS

We have investigated structural and dynamical as well as optical properties of charge-stabilized colloidal suspensions. Provided that the interaction potential is sufficiently screened (as it is in our case), the system can be described as a suspension of hard spheres. Different static and dynamic aspects of these materials have been addressed. Using small-angle neutron scattering, we have determined the static structure factor  $S(q)$  which is found in excellent agreement with integral equation theory for a suspension of hard spheres. Our results show once again that SANS is an ideal tool to study the structural properties of dense suspensions at any volume fraction if the solvent scattering length density (a water-deuterium mixture) is properly chosen in order to avoid multiple (neutron) scattering. Compared to light scattering, SANS offers particular advantages for strongly turbid systems and allows measurements at large  $q$  values, difficult to access otherwise. In comparison to high flux x-ray scattering [49] SANS is absolutely nondestructive. Based on the measurements of  $S(q)$ , we compared the optical density of our colloidal systems to the theoretical predictions and good agreement is found as well. We conclude that even in the case of particles much smaller than the wavelength of light, the theoretical concepts to describe photon diffusion apply quantitatively. We have furthermore shown that a full structural characterization provides an excellent basis for the study of local particle dynamics using DWS. Finally, we have addressed the influence of structural correlations on the polarization properties of multiply scattered light and its impact on DWS experiments. The observed strong concentration dependence can be explained in terms of the modified single-scattering properties due to the local structural order.

Our results demonstrate that a combination of SANS and DWS is a method perfectly suited for the study of structural and dynamic as well as optical properties of dense particle systems. Future experiments will address more complex structures and interaction potentials, both attractive and repulsive, which may allow us to elucidate the general effect of direct and indirect interactions on the macroscopic properties of these interesting materials.

## ACKNOWLEDGMENTS

F.S. would like to thank Ralf Lenke and Georg Maret for discussions. The small-angle neutron scattering (SANS) experiments were carried out at the Paul Scherrer Institute (P.S.), Villigen (Switzerland). We are particularly indebted to Joachim Kohlbrecher (PSI) for help and assistance using the SANS facility. We gratefully acknowledge financial support from the Swiss National Science Foundation.

- [1] See, e.g., W.B. Russel, D.A. Saville, and W.R. Schowalter, *Colloidal Dispersion* (Cambridge University Press, Cambridge, U.K., 1989).  
 [2] P.N. Segré, S.P. Meeker, P.N. Pusey, and W.C. Poon, *Phys. Rev. Lett.* **75**, 958 (1995).  
 [3] A.P. Gast and W.B. Russel, *Phys. Today* **51**(12), 24 (1998).

- [4] A.D. Dinsmore, A.G. Yodh, and D.J. Pine, *Phys. Rev. E* **52**, 4045 (1995).  
 [5] S. Romer, F. Scheffold, and P. Schurtenberger, *Phys. Rev. Lett.* **85**, 4980 (2000).  
 [6] K. Dawson *et al.*, *Phys. Rev. E* **63**, 011401 (2000).  
 [7] P.N. Pusey and R.J.A. Tough, in *Dynamic Light Scattering:*

- Applications of Photon Correlation Spectroscopy*, edited by R. Pecora (Plenum Press, New York, 1981).
- [8] P. Schurtenberger and M.E. Newman, in *Environmental Particles*, edited by J. Buffle and H.P. van Leeuwen (Lewis Publishers, Boca Raton, FL, 1993), Chap. 2, pp. 37–115.
- [9] G. Maret and P.E. Wolf, *Z. Phys. B: Condens. Matter* **65**, 409 (1987).
- [10] D.J. Pine, D.A. Weitz, P.M. Chaikin, and E. Herbolzheimer, *Phys. Rev. Lett.* **60**, 1134 (1988).
- [11] D.A. Weitz and D.J. Pine, in *Dynamic Light Scattering*, edited by W. Brown (Oxford University Press, New York, 1993), Chap. 16, pp. 652–720.
- [12] D.A. Weitz, J.X. Zhu, D.J. Durian, and D.J. Pine, in *Structure and Dynamics of Strongly Interacting Colloids and Supramolecular Aggregates in Solution*, edited by S.-H. Chen, J. S. Huang, and P. Tartaglia (Kluwer Academic Publishers, Dordrecht, 1992), p. 731.
- [13] M.H. Kao, A.G. Yodh, and D.J. Pine, *Phys. Rev. Lett.* **70**, 242 (1993).
- [14] S. Romer, C. Urban, V. Lobaskin, A. Stradner, F. Scheffold, J. Kohlbrecher, and P. Schurtenberger (unpublished).
- [15] J.P. Hansen and I.R. McDonald, *Theory of Simply Liquids* (Academic Press, London, 1986).
- [16] G. Jerke, J.S. Pedersen, S.U. Egelhaaf, and P. Schurtenberger, *Langmuir* **14**, 6013 (1998).
- [17] J.P. Cotton, in *Initial Data Treatment, in Neutron, X-Ray and Light Scattering: Introduction to an Investigative Tool for Colloidal and Polymeric Systems*, edited by P. Lindner and T. Zemb (North-Holland, Amsterdam, 1989).
- [18] B. Jacrot and G. Zaccai, *Biopolymers* **20**, 2413 (1981).
- [19] M. Ragnetti and R.C. Oberthür, *Colloid Polym. Sci.* **264**, 32 (1986).
- [20] G.D. Wignall and F.S. Bates, *J. Appl. Crystallogr.* **20**, 28 (1987).
- [21] J.S. Pedersen, D. Posselt, and K.J. Mortensen, *J. Appl. Crystallogr.* **23**, 321 (1990).
- [22] J.G. Barker and J.S. Pedersen, *J. Appl. Crystallogr.* **28**, 105 (1995).
- [23] P. R. Bevington, *Data Reduction and Error Analysis for the Physical Sciences* (McGraw-Hill, New York, 1969).
- [24] M.P. van Albada and A. Lagendijk, *Phys. Rev. Lett.* **55**, 2692 (1985); P.E. Wolf and G. Maret, *ibid.* **55**, 2696 (1985).
- [25] F. Scheffold and G. Maret, *Phys. Rev. Lett.* **81**, 5800 (1998).
- [26] *Scattering and Localization of Light in Random Media*, edited by P. Sheng (World Scientific, Singapore, 1990).
- [27] P.W. Anderson, *Philos. Mag. B* **52**, 505 (1985).
- [28] D.S. Wiersma, P. Bartolini, A. Lagendijk, and R. Rhigini, *Nature (London)* **390**, 671 (1997); F. Scheffold, R. Lenke, R. Tweer, and G. Maret, *ibid.* **398**, 206 (1999).
- [29] S. Fraden and G. Maret, *Phys. Rev. Lett.* **65**, 512 (1990); X. Qiu, X.L. Wu, J.Z. Xue, D.J. Pine, D.A. Weitz, and P.M. Chaikin *ibid.* **65**, 516 (1990); P.D. Kaplan, A.G. Yodh, and D.J. Pine, *ibid.* **68**, 393 (1992).
- [30] P.M. Saultier, M.P. Zinkin, and G.H. Watson, *Phys. Rev. B* **42**, 2621 (1990).
- [31] A. Dogariu, C. Kutsche, P. Likamwa, G. Boreman, and B. Moudgil, *Opt. Lett.* **22**, 585 (1997).
- [32] H. C. van de Hulst, *Light Scattering by Small Particles* (Dover, New York, 1981); C. F. Bohren and D. R. Huffman, *Absorption and Scattering of Light by Small Particles* (John Wiley & Sons, New York, 1983).
- [33] A. Ishimaru, *Wave Propagation and Scattering in Random Media* (Academic Press, New York, 1978).
- [34] P.D. Kaplan, A.D. Dinsmore, A.G. Yodh, and D.J. Pine, *Phys. Rev. E* **50**, 4827 (1994).
- [35] E.J.W. Verwey and J.T.G. Overbeek, *Theory of the Stability of Lyophobic Colloids* (Elsevier, Amsterdam, 1948).
- [36] C.W.J. Beenakker and P. Mazur, *Physica (Amsterdam)* **126A**, 349 (1984).
- [37] F. Scheffold, S.E. Skipetrov, S. Romer, and P. Schurtenberger, *Phys. Rev. E* **63**, 061404 (2001).
- [38] S.J. Nilsen and A.P. Gast, *J. Chem. Phys.* **101**, 4975 (1994).
- [39] Here  $P(q)$  denotes the Mie scattering function of a single particle while the (different) SANS particle form factor, introduced in Sec. III B, is called  $F(q)$ .
- [40] We have verified by a full analysis of Eq. (11) [with  $h(q) = h(q, t)$ ] that under the chosen experimental conditions, contributions from intermediate and long times are dominant in Eq. (11), hence our assumption  $h(q, t) \cong h(q, \infty) = h(q)$  is justified.
- [41] G.K. Batchelor, *J. Fluid Mech.* **74**, 1 (1976).
- [42] A.J.C. Ladd, H. Gang, J.X. Zhu, and D.A. Weitz, *Phys. Rev. Lett.* **74**, 318 (1995); *Phys. Rev. E* **52**, 6550 (1995).
- [43] E. Akkermans, P.E. Wolf, R. Maynard, and G. Maret, *J. Phys. (France)* **49**, 77 (1988).
- [44] A finite sample cell and/or the presence of absorption leads to a rounding of the correlation function at short correlations time. In our case these contributions are small (as can be seen in Fig. 6) and hence do not affect the slope of  $\ln(g_1(\sqrt{t}))$ . For details, see Ref. [11].
- [45] F.C. MacKintosh and Sajeev John, *Phys. Rev. B* **40**, 2383 (1989).
- [46] F.C. MacKintosh, J.X. Zhu, D.J. Pine, and D.A. Weitz, *Phys. Rev. B* **40**, 9342 (1989).
- [47] D.A. Zimnyakov, Y.P. Sinichkin, P.V. Zakharov, and D.N. Agafonov, *Waves Random Media* **11**, 395 (2001).
- [48] H. Wyss, S. Romer, F. Scheffold, P. Schurtenberger, and L.J. Gauckler, *J. Colloid Interface Sci.* **241**, 89 (2001).
- [49] D.O. Riese, W.L. Vos, G.H. Wegdam, F.J. Poelwijk, D.L. Abernathy, and G. Grübel, *Phys. Rev. E* **61**, 1676 (2000).